АННОТАЦИЯ к статье

A.P.Safronov, I.V.Beketov, I.S.Tyukova, A.I.Medvedev, O.M.Samatov, A.M.Murzakaev
Magnetic nanoparticles for biophysical applications synthesized by high-power physical dispersion. J. Magn. Magn. Mat. 2015. DOI 10.1016/j.jmmm.2014.11.016
Elsevier, 2015

Малозатратные и высокопроизводительные методы высоко-энергетического физического диспергирования: электрический взрыв проволоки и лазерное испарение мишени были использованы для получения магнитных наночастиц оксида железа (МНЧ) с контролируемыми параметрами дисперсности и воспроизводимыми функциональными свойствами. Синтезированные МНЧ были сферической формы, имели средний размер 10-30 нм и узкое распределение по размерам. Фазовый состав, форма, размер частиц и функциональные свойства МНЧ были исследованы набором современных экспериментальных методов. Вследствие неравновесных условий получения фазовый состав МНЧ отвечает не магнетиту, а маггемиту. В то же время магнитные свойства МНЧ являются воспроизводимыми и близки к супер-парамагнетизму однодоменных частиц. Хотя получаемые МНЧ являются агрегированными в воздушно-сухом состоянии, их де-агрегирование может быть успешно проведено в жидкой среде. Также может быть проведена модификация поверхности частиц. Показано, что суспензии получаемых МНЧ являются стабильными в широком диапазоне внешних условий и могут применяться для биофизических целей

MAGNETIC NANOPARTICLES FOR BIOPHYSICAL APPLICATIONS SYNTHESIZED BY HIGH-POWER PHYSICAL DISPERSION

A.P.Safronov[a], I.V.Beketov[a,b], I.S.Tyukova[a], A.I.Medvedev[a,b], O.M.Samatov[b], A.M.Murzakaev[b]

[a]Ural Federal University, Yekaterinburg, Russia

[b]Institute of Elecrophysics, Ural branch of RAS, Yekaterinburg, Russia

Safronov@iep.uran.ru

Abstract

The low cost and high output methods of high-power physical dispersion: the electrical explosion of wire and the laser target evaporation were elaborated for the production of iron oxide magnetic nanoparticles (MNPs) with controlled dispersion parameters and highly reproducible functional properties. The synthesized MNPs were spherical in shape with mean diameter 10 nm and lognormal particle size distribution. The phase composition, shape, particle size and functional properties of MNPs were cross-examined by a variety of contemporary experimental techniques. The phase structure of MNPs corresponds to inverse spinel of magnetite. Meanwhile, due to the non-equilibrium conditions of the dispersion chemical composition of MNPs is close to maghemite – γ-Fe_2O_3. Their magnetic properties are reproducible and very close to the single domain superparamagnetic behavior. The stability of the suspensions of these MNPs and their applicability in the biophysical purposes such magneto-induced heating has been demonstrated.

Keywords: iron oxide**,** nanoparticles, stabilization of suspensions, magneto-induced heating

1. Introduction

The biomedical application of magnetic nanoparticles (MNPs) is at the leading edge of the developing field of nanotechnology. A variety of promising schemes for the application MNPs include magnetically induced drug delivery, magnetic biosensing, magnetic resonance imaging, cancer diagnostics and therapy by hyperthermia, cell markers, magnetically driven actuators etc [1-4]. Magnetically active iron oxides – magnetite and maghemite take the leading role among other MNPs potentially suitable for the biomedical applications. The most common route to biomedical magnetite MNPs now is the chemical precipitation from the mixture of ferrous and ferric chlorides. It gives the chemically stable but irregularly shaped monocrystalline MNPs with different particle size depended on the synthesis conditions. Magnetite MNPs for biomedical applications usually are synthesized by the precipitation from the mixture of ferric and ferrous salts in their aqueous

solutions at high pH and at elevated temperatures [5,6]. The state of the art of this procedure is to obtain uniformly dispersed individual magnetite nanoparticles. Although it is certainly achievable not only in the lab, but also in the industry, the process of chemical synthesis is not easy to control. Thus, it is difficult to maintain batch to batch reproducibility of the product, especially if it comes to the industrial technology. Therefore, the necessity for the alternative ways for the fabrication of iron oxide MNPs for the prospective biophysical and biomedical application does not vanish. The today demands of the development of the nanomedicine are the high output methods of synthesis of low-cost MNPs with the controllable and reproducible properties [7]. Physical methods of the dispersion of solids in the gas phase by the high-energy impact exactly meet these requirements.

In the present study we have synthesized iron oxide MNPs by two the most productive methods of high-temperature physical dispersion – the electrical explosion of wire (EEW) and the laser target evaporation (LTE). The comparable structural and magnetic characterization of the obtained MNPs was performed. To facilitate the prospective biophysical application of MNPs, the stability of their aqueous suspensions was studied. Direct isothermal calorimetry was elaborated for the magneto-inductive heating experiments of the MNPs suspensions.

2. Experimental part

2.1 Methods of MNPs preparation

The electrical explosion of wire (EEW) [8] is based on the evaporation of the portion of the metallic wire by the high-voltage pulse. Originated from the simple electrical fuse, which cuts off the electrical circuit under the overload, now it becomes state of the art technique, which can give 10^2 - 10^3 g of spherically shaped metal and metal oxide nanoparticles per 1 h. If the high-power electrical direct current (DC) passes through the metal wire, it is overheated and explodes, giving the cloud of the metal vapors at the temperature around 10^4 K. The vapors rapidly expand in the cold surrounding gas and condense there. Due to the high speed of the expansion the concentration of vapors is low and they condense in the shape of spherical particles. EEW was performed in the the oxidizing gas mixture ($79\%N_2+21\%O_2$) using the iron wire 0.5 mm in diameter in 220 mm portions continuously fed from the roll. The iron vapors oxidized during the expansion and gave iron oxide MNPs. The permanent gas flow was maintained in the EEW installation, the obtained nanoparticles were moved out from the explosion zone, and collected in the filter section of the apparatus. The EEW process was performed in a continuous step-wise way provided high production rate of MNPs. More details of EEW method and its experimental setup are given elsewhere [9].

In the laser target evaporation (LTE) the overheating of the solid is achieved by the high-power pulse of laser beam focused on the flat surface of the pressed solid pellet. The energy introduced provides burst-like evaporation in the laser spot on the surface. Extra energy of the laser beam is transferred into the kinetic energy of the vapors, which are rapidly ejected away from the surface. The pressed pellet for the LTE was made of the commercial Fe_2O_3 (Alfa Aesar). The evaporation chamber was filled by the flowing gas mixture ($79\%N_2+21\%O_2$). To provide the continuous evaporation of the iron oxide the pellet rotated. Additionally it was linearly shifted in the direction perpendicular to the axis of rotation to achieve the spiral trace of the laser beam at the upper surface of the pellet. More details of LTE method and its experimental setup are given elsewhere [10].

The iron oxide MNPs obtained in this study by EEW and LTE methods are further designated EEW-NP and LTE-NP.

2.2 Methods of MNPs characterization

The X-ray diffraction (XRD) studies were performed by operating at 40kV and 40 mA DISCOVER D8 (Bruker) diffractometer using Cu-Kα radiation (λ = 1.5418 Å), a graphite monochromator and a scintillation detector. Bruker software TOPAS-3 with Rietveld full-profile refinement was employed for the quantitative analysis of all the diffractograms. TEM was performed using a JEOL JEM2100 microscope operating at 200 kV. The specific surface area (S_{sp}) of MNPs was measured by the low-temperature sorption of nitrogen (Brunauer-Emmett-Teller physical adsorption (BET)) using Micromeritics TriStar3000 analyzer. The stoichiometric ratio Fe^{2+}/Fe^{3+} in the MNPs was determined by Red-Ox potentiometric titration under an argon atmosphere by potassium dichromate using an automatic titrator TitroLine (Schott Instruments). Magnetic measurements were performed by a vibrating sample magnetometer (Cryogenics Ltd. VSM).

2.3 Preparation of MNPs suspensions

The aqueous suspensions were prepared by the dispersion of air-dry iron oxide MNPs in distilled water at 298 K. Typically the stock suspension with concentration of MNPs 50 g/L was first prepared and then it was diluted to the necessary level. The stock suspension was de-aggregated in the same way as described in our previous reports [10]. Two types of de-aggregated suspensions were obtained: the first one was a water based suspension without electrostatic stabilizer and the second one was a water based suspension with Na citrate (0.05M) as an electrostatic stabilizer.

2.4 Methods of characterization of suspensions

Aggregation of MNPs in water suspension was studied by dynamic light scattering (DLS) using the Brookhaven ZetaPlus particle size analyzer. The electrokinetic zeta-potential of the suspensions was measured by electrophoretic light scattering (ELS) using the same analyzer. All the measurements were made at 298 K in suspensions diluted down to 0.1 g/L by distilled water. Ultrasound treatment of the suspensions for the de-aggregation was performed using a Cole-Palmer CPX-750 processor at a 300 W average power output level. Centrifuging of the suspensions was performed using a Hermle Z383 centrifuge with a 218 rotor at a maximum of 15 000 rpm.

Calorimetric measurements of the magneto-induced heating of the suspensions were performed using isothermal 3D Calvet differential calorimeter SETARAM C80. Two identical magnetic coils (length 70 mm, outer diameter 10 mm) were placed in the cells of the calorimeter. The coil consisted of four wire layers with the loop density 3000 loops per 1 m. Both coils were in the serial connection to the commercial sound wave generator G3-109 (Etalonpribor, Russian Federation) . The standard resistance 1 Ohm was serially connected to the circuit and the voltage drop on it was measured by Tecktronix TDS1012 oscilloscope. 150 mA - current intensity, sine-wave - the shape of the wave, 212 kHz - frequency of the alternating current (AC). The glass vial 1 mL in volume was placed inside each coil. One of the coils contained the vial with the suspension of MNPs, another coil with an empty vial was the reference for the calorimetric experiment.

3. Results and discussion

3.1 Characterization of iron oxide MNPs

Fig. 1 presents TEM images of EEW-NPs and LTE-NPs. The particles are spherically shaped. The particle size distribution (PSD) by number is lognormal for both samples (Fig. 2). The medians of lognormal PSD are very close for both samples but the lognormal dispersion (Table 1) is substantially higher for EEW-NPs. LTE provides narrower PSD than EEW.

The specific surface area of the spherically shaped particles can be used for the calculation of the surface average diameter (d_S) , which equals to $6/(S\rho)$ [11], S being the specific surface area and ρ – the density of MNPs. The values of d_S calculated from the PSD are very close to the values obtained from the specific surface of MNPs (given in brackets)

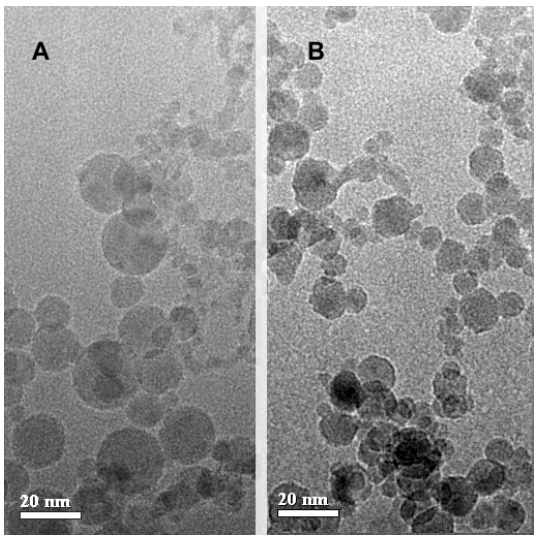

Figure 1. TEM images of EEW-NPs (A) and LTE-NPs (B).

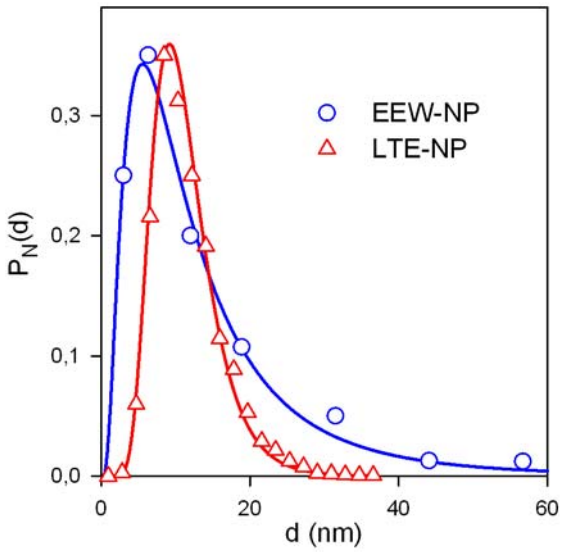

Figure 2. Particle size distributions (by number) of iron oxide MNPs.

Table 1

Selected parameters of iron oxide MNPs

Parameter	EEW-NP	LTE-NP
Median of PSD, nm	10.5	10.5
Lognormal dispersion of PSD	0.432	0.368
Specific surface area, m^2/g	86	93

Surface average diameter d_S, nm	16.7 (15.5)[a]	14.7 (14.4)[a]
Crystalline phases	Magnetite 93.6% Hematite 6.4%	Magnetite 100%
Coherent length, nm	33	10
Lattice period, A	8.368	8.358
Chemical composition	$Fe_{2.70}O_4$	$Fe_{2.68}O_4$
Saturation magnetization[b] at 298 K, emu/g	55	46

[a] calculated from the specific surface area

[b] At 10 T field

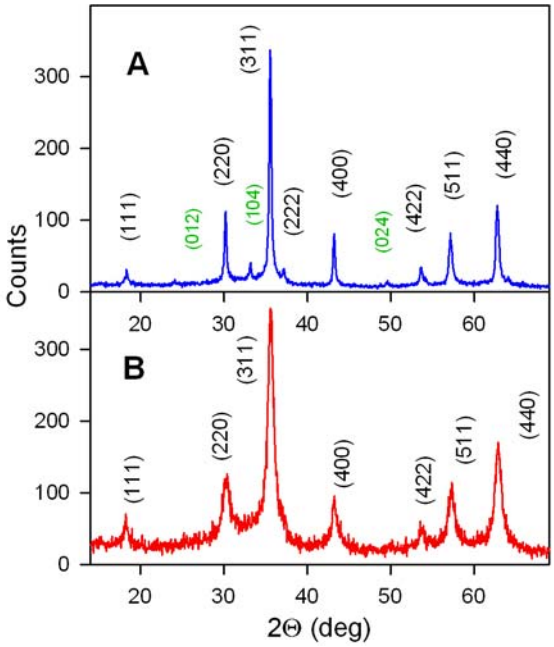

Figure 3. XRD patterns for EEW-NP (A) and LTE-NP (B). Black indexes for magnetite. Green indexes for hematite.

Fig. 3 presents XRD patterns for the iron oxide MNPs. The experimental points are fitted well by the magnetite XRD database. In addition to the magnetite phase EEW-NP contains minor fraction of hematite. It is well known that based only on XRD data magnetite (Fe_3O_4) structure can not be distinguished from maghemite (γ-Fe_2O_3) [12]. The crystalline cell of both oxides corresponds

to the inverse spinel structure with space group Fd3m [13]. Although the crystalline structures of magnetite and maghemite are basically the same, the Fe^{3+} cations are slightly smaller than Fe^{2+} cations, and, hence, the lattice period of maghemite (0,8346) is a little bit lower than that of magnetite (0,8396) [14]. The XRD parameters for MNPs given in Table 1 show that the lattice periods of the crystalline phase both for EEW-NPs and LTE-NPs are substantially lower as compared to that of stoichiometric magnetite Fe_3O_4 but higher than the lattice period of maghemite γ-Fe_2O_3.

The chemical composition of LTE MNPs was determined by the Red-Ox titration. The non-stoichiometry with regard to magnetite was calculated from the titrated amount of Fe^{2+} and the total amount of Fe in MNPs. The chemical composition of MNPs found by Red-Ox titration is given in Table 1. Thus, based on XRD and chemical analysis we concluded that iron oxide MNPs synthesized by EEW and LTE both had got inverse spinel structure which is very close to maghemite but contained slightly less number of cation vacancies per cell.

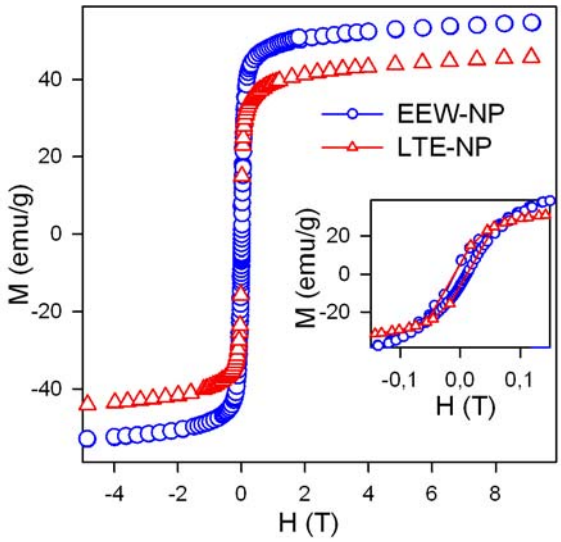

Figure 4. Hysteresis loops of iron oxide MNPs at 300 K. Inset – enlarged view for the low fields.

Fig. 4 presents the hysteresis loops for the iron oxide MNPs. One can see no saturation even in the high magnetic fields. It is one of the features of the superparamagnetic behavior, which might be anticipated for the spherical iron oxide MNPs with the average particle size around 10 nm. In the high fields the magnetization of EEW-NPs is higher than LTE-NPs but in both cases it is lower than for the pure maghemite 82 emu/g [15]. The shape of the hysteresis loops for EEW-NPs and LTE-NPs is almost identical and is very close the Langevin function which characterizes the superparamagnetic behavior [16]. However, there is still some deviation from the superparamagnetc behavior revealed by comparative analysis of hysteresis loops measured for different temperatures and zero-field cooled and field cooled thermomagnetic curves. The specific features of the magnetic

behavior of LTE-Nps were in detail discussed in ref [9]. It was shown that it fits well the core-shell model which combines the ferrimagnetic maghemite core with the anisotropy field 20 kA/m and the shell of frozen spins, which lacks long-range magnetic order yielding spin glass. The estimation of the thickness of the shell gives 0.6 – 1.2 nm. The bulk to shell ratio is higher in case of EEW-NP and it provides higher magnetization values.

3.2 Stability of iron oxide MNPs suspensions

Iron oxide MNPs synthesized by EEW and LTE easily give stable suspension in water. The specific feature of the dispersion is the self-stabilization of the suspensions [9], i.e. no special stabilizer is needed to provide aggregation and sedimentation stability of the suspension. The basic mechanism of stabilization is the formation of the double electrical layer on the surface of the dispersed MNPs. The zeta-potential of EEW-NP and LTE-NP suspensions determined by the electrophoretic light scattering is around +40 mV. Alternative to the electrostatic self-stabilization of EEW-NP and LTE-NP suspensions, which give positively charged MNPs, the typical electrostatic stabilizers may as well be used for the stabilization. For example, sodium citrate, being added in 0.05M concentration, provides stable suspensions with negative value of zeta-potential (-40 mV). Thus, EEW-NP and LTE-NP suspensions can be stabilized by versatile ways, providing either negatively or positively charged MNPs.

Concerning the biomedical application the most important is the stability of suspensions in physiological solutions, which contain large concentration of salts. The salts increase the ionic strength of the medium, and it is very unfavorable to the electrostatic stabilization of the suspensions. The influence of salt on the stability of LTE-NP suspensions is shown in Fig. 5, which presents the dependence of the hydrodynamic diameter of aggregates in the suspension and its zeta-potential on the concentration of sodium chloride. Zeta-potential both for self-stabilized and for citrate-stabilized suspensions linearly decreases with the logarithm of the molar concentration of sodium chloride. It indicates the diminishing of the electrostatic stabilization of the suspension. It becomes almost zero at the physiological concentration of NaCl, which is around 0.2 M in human blood. As the stabilization of the suspension vanishes, the aggregation of MNPs begins. However, it goes differently for the self-stabilized and citrate-stabilized suspensions. In the former case the hydrodynamic diameter gradually increases with salt concentration. In the latter case the diameter stays almost constant in the wide concentration range and steeply increases at high NaCl content. It indicates that the citrate-stabilized LTE-NP suspension still keeps the stability despite the lack of electrostatic repulsion between particles. Thus, the stabilization by citrate is more suitable for the biomedical application of MNPs than their self-stabilization, likely because the adsorbed citrate

provides the protective steric shell, which prevents the aggregation of MNPs. However, this shell can stand salt concentration only at lower physiological limit. To provide the stability of MNPs suspension in the broad range of salt concentration steric stabilization by polymeric shells is necessary.

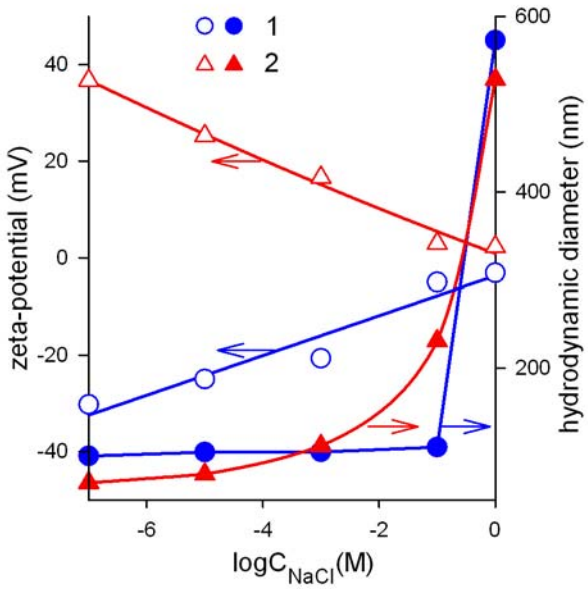

Figure 5. The influence of salt on the hydrodynamic diameter and zeta potential in LTE-NP suspensions. 1 – citrate stabilization. 2 – self-stabilization.

Such stabilization can be provided by the chitosan – the chemical derivative of the natural polysaccharide – chitin. Chitosan is well-known as a biocompatible polymeric modifier of iron oxide MNPs for the biomedical applications [17]. Chitosan is the polycationic polymer: its monomeric units contain amine groups, which can bind protons in the acidic solutions and provide the positive electrical charge on the macromolecules. The value of the total charge located on the chitosan chains is pH-dependent. It is high at low pH and vanishes with the increase of pH.

We have used commercially available chitosan (Mirra, Schelkovo, Russian Federation) with M = 120 KDa and deacetilation degree 65.0% to modify LTE-NP suspensions stabilized by citrate. These suspensions were mixed in equal proportions with 0.4% of chitosan solution in 0.2 M hydrochloric acid. The stability of the obtained polymer-colloid suspensions to the addition of salt (NaCl) was studied at two pH values: in acidic solution (pH=1.8) and at pH=6.8 close to physiological levels.

Fig. 6 presents the dependence of the hydrodynamic diameter of the modified MNPs and zeta-potential on the concentration of NaCl. At low NaCl concentration at pH=1.8 the hydrodynamic diameter is low and zeta-potential is high. It means that the suspension is effectively stabilized due to the adsorption of ionized chitosan macromolecules on MNP surface. However, upon the addition

of salt in the acidic solution zeta-potential vanishes, the suspension is de-stabilized, and the hydrodynamic diameter steeply increases. If salt is added at pH=6.8 the initial hydrodynamic diameter is higher that at low pH, but it maintains stability over the entire range of salt concentration. Zeta-potential at pH=6.8 is lower that at pH=1.8 and decreases with salt concentration in a similar way. It means that it is not the electrostatic repulsion, which provides stability of the suspension modified by chitosan. It is important that the suspension of MNPs was first mixed with the acidic solution of chitosan, and then polymer-colloid suspension neutralized to pH=6.8. If the suspension was mixed with the chitosan solution pre-neutralized to pH=6.8, no stability to elevated salt concentration was observed.

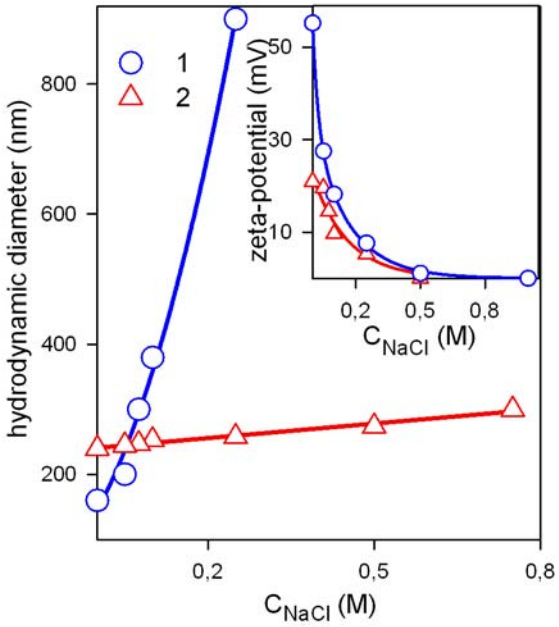

Figure 6. The influence of salt concentration on the hydrodynamic diameter and zeta-potential (inset) of chitosan-modified MNPs. 1 – pH=1.8. 2 – pH=6.8.

Thus the modification of MNPs by chitosan goes in steps. On the first step citrate-stabilized MNPs suspension is mixed with the acidic solution of chitosan. At low pH chitosan molecules are ionized and have expanded conformations due to the electrostatic repulsion of charged monomeric units. The expanded positively charged macromolecules readily adsorb onto the negatively charged surface of MNPs. If pH is increased, chitosan polycations are neutralized and cuddle to the more compact conformation encapsulating MNPs inside the shell (Fig. 7).

The hydrodynamic diameter of the encapsulated particle enlarges due to the thick polymeric layer on the surface. Such encapsulated particles are very resistant to the addition of salts. In case if the neutralization of chitosan is performed before mixing with MNPs, macromolecules take compact uncharged conformation first and can not absorb onto MNPs.

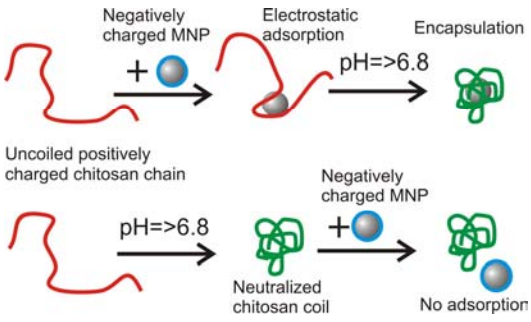

Figure 7. Encapsulation of LTE-NPs by chitosan. Upper scheme – MNPs suspension is first mixed with acidic chitosan solution and then neutralized to pH=6.8. It provides encapsulation of MNPs. Lower scheme – chitosan solution is first neutralized to pH=6.8 and then mixed with MNPs suspension. No stabilization is achieved.

3.3 Magneto-induced heating of LTE-NP suspension

We have used low fields, which are much easily obtained, and have elaborated the direct isothermal Calvet calorimetry [18] to study the magneto-induced heating of MNPs suspension. The measured quantity in the method is the heat flux from the calorimetric cell. We have placed the magnetic coil inside a calorimetric cell and have measured directly the evolution of heat from the suspension. In these experiments we tested LTE-NP suspension with 4.56% weight concentration of iron oxide.

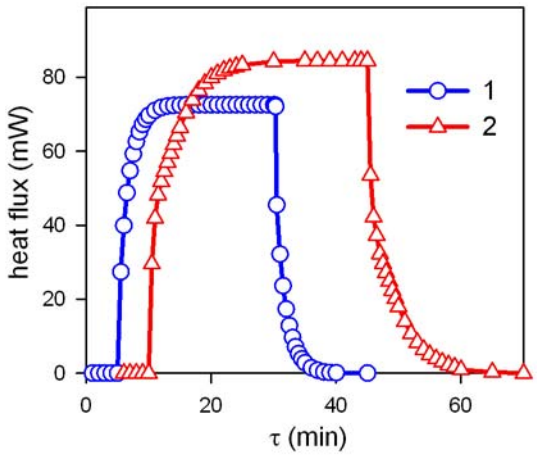

Figure 8. Time dependence of the heat flux from the empty coil (1) and from the coil with ferrofluid (2). H=15.1Oe. C=4.56%. m=0.596 g.

Fig. 8 presents the time course of the heat flux from the coil with the LTE-NP ferrofluid in comparison with the empty coil. If no current is applied to the coil the calorimeter shows the baseline. When the current is switched on, the calorimeter cell begins to heat up and the signal

increases to the saturation with the rate dependent on the heat capacity of the cell. Eventually the heat equilibrium is established and the measured heat flux from the cell becomes equal to the heat power evolved by the magnetic field. It is clear from Fig. 8 that the heat flux from the coil with the ferrofluid is higher than the heat flux from the empty coil. The difference relates to the magneto-induced heating of the suspension. At the end of the experiment the current is switched off, the heat evolution in the coil stops and the heat flux decreases to the initial baseline.

The measured values of the specific power loss for the LTE-NP suspension were compared with the theoretical estimation for the ensemble of spherical single domain magnetic particles given by the equation:

$$P = \frac{\mu_0^2 \omega H^2 M_s^2 V}{3\rho k_B T} \frac{\omega\tau}{1+\omega^2\tau^2} \quad (1)$$

μ_0 – the magnetic permeability of vacuum, ω – field frequency, H – field strength, M_s – saturation magnetization of LTE-NP (Table 1), V, ρ – volume and density of LTE-NP, k_B – Boltzmann constant, τ – relaxation time.

There are two basic mechanisms of the dipole relaxation in the field: Neel relaxation due to the reorientation of the dipole in the crystal lattice of the single domain particle and Brownian relaxation due to the rotation of the particle in the field. Neel relaxation is typical for the particles in the 2 – 6 nm range, while Brownian relaxation dominates for the ensembles of larger particles. Considering the PSD of LTE-NP (Fig. 2) and the average values of particle size (Table 1) we evaluated relaxation time of LTE-NPs in Brownian mode according the equation

$$\tau = \frac{4\pi\eta R^3}{k_B T} \quad (2)$$

R – average radius of LTE-NPs (half of the diameter given in Table 1)

Fig. 9 presents the frequency dependence of the experimental values of the magneto-induced heat power per 1 g of LTE-NP (points). They are in a good agreement with the theoretical evaluation by Equation (1) (lines).

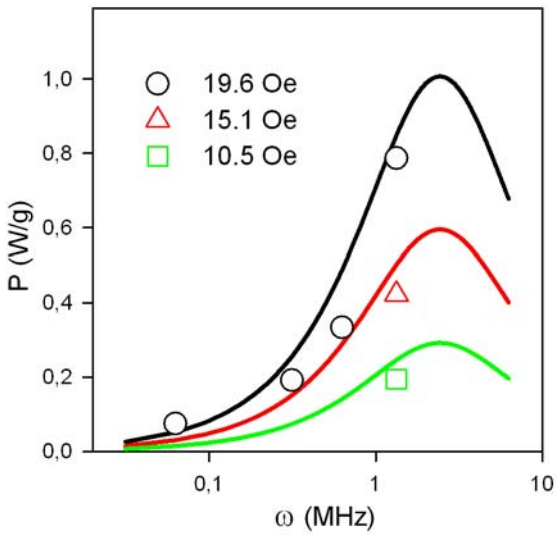

Figure 9. Frequency dependence of the specific loss power of LTE-NP ferrofluid. Points – experiment. Lines – the theory.

4. Conclusions

The low cost and high output methods of the thermal physical dispersion: the electrical explosion of wire (EEW) and the laser target evaporation (LTE) were elaborated for the synthesis of iron oxide MNPs with spherical shape and average diameter 10 nm. The MNPs obtained by EEW and LTE are very similar in phase composition, magnetic characteristics, and the properties of the water suspensions. They differ only in their particle size distribution, which in narrower in the case of LTE. Due to the non-equilibrium conditions of the high-temperaure condensation of vapors the phase structure of MNPs corresponds to maghemite rather than magnetite. Meanwhile, their magnetic properties are reproducible and very close to the single domain super-paramagnetic behavior. Although the as-prepared MNPs are initially aggregated in the air-dry state their de-aggregation in liquid suspension can be successfully performed. The stability of the suspensions can be achieved either by self-stabilization giving positively chaged MNPs, or by using citrate stabilizer, which provides negative charge on the particles. Electrostatic stabilization of both types is however not efficient to maintain stability of the MNPs in the salt solutions in the physiological range of concentration. It can be achieved by the encapsulation of MNPs in the shell of biocompartible polymer - chitosan. The magneto-induced heating of the MNPs suspesion is in a good agreement with the theoretical consideration based on the Brownian relaxation mode.

Acknowledgement

The research was done with the financial support of the Russian Science Foundation grant 14-19-00989.

References

[1] S. Mournet, S. Vasseur, F. Grasset, E. Duguet, J. Mater. Chem. 14 (2004) 2161.

[2] R. Hergt, S. Dutz, R. Muller, M. Zeisberger, J. Phys.: Condens. Matter. 18 (2006) S2919.

[3] J. Llandro, J. J. Palfreyman, A. Ionescu, and C. H. W. Barnes, Med. Biol. Eng. Comput. 48 (2010) 977.

[4] G.V. Kurlyandskaya, J. Magn. Magn. Mater., 321 (2009) 659.

[5] B. Berkowski (ed) Magnetic Fluids and Application Handbook, Begell House: UNESCO, 1996

[6] J. C. Aphesteguy, S. E. Jacobo, N. N. Schegoleva and G. V. Kurlyandskaya, Journal of Alloys and Compounds, 495 (2010) 509.

[7] J. H. Grossman, S. E. McNeil, Physics Today. 65 (2012) 38.

[8] Yu. A. Kotov, J. Nanopart. Res. 5 **(**2003) 539.

[9] G. V. Kurlyandskaya, S. M. Bhagat, A. P. Safronov, I. V. Beketov, A. Larranaga, AIP Advances. 1 (2011) 042122.

[10] A. P. Safronov, I. V. Beketov, S. V. Komogortsev, G. V. Kurlyandskaya, A. I. Medvedev, D. V. Leiman, A. Larranaga, S. M. Bhagat AIP Advances. 3 (2013) 052135.

[11] P. C. Hiemenz, R. Rajagopalan, Principles of Colloid and Surface Chemistry. Marcel Dekker, New York. 1997.

[12] I. S. Lyubutin, C. R. Lin, Yu. V. Korzhetskiy, T. V. Dmitrieva, R. K. Chiang, J. Appl. Phys. 106 (2009) 034311.

[13] J. B. Goodenough, Magnetism and the Chemical Bond. Interscience, New York, 1963.

[14] W. B. Pearson Handbook of lattice spacing structures of metals and alloys. London. Pergamon Press. 1958.

[15] E. Muller, Ch. Oestreich, U. Popp, G. Michel, G. Staupendahl, K.-H. Henneberg, J. KONA-Powder and Particle (Osaka), 13 (1995) 79.

[16] R. C. O'Handley, Modern Magnetic Materials. John Wiley & Sons, New York, USA, 1972.

[17] J. Qu, G. Liu, Y. Wang, R. Hong, Advance Powder Technology 21 (2010**)** 461.

[18] E. Calvet, H. Prat, H. Skinner, Recent progress in microcalorimetry, Pergamon Press, Oxford, London, New York, Paris, 1963.